MOLEKUL
www.jmolekul.com

Articles

https://doi.org/10.20884/1.jm.2021.16.1.644

Purification of Carbon-Based Magnetic Nanoparticles (CMNs) Produced by Submerged Arc Discharge in Liquid Ethanol/Ethylenediamine

Oktaviana Dyah Mayasari, Dielsa Eka Kuswari, Witri Wahyu Lestari, Teguh Endah Saraswati*

Department of Chemistry, Faculty of Mathematics and Natural Sciences, Sebelas Maret University, Jl. Ir. Sutami No.36A, Surakarta, 57126, Indonesia

*Corresponding author email: teguh@mipa.uns.ac.id

Received February 13, 2020; **Accepted** November 27, 2020; **Available online** March 25, 2021

ABSTRACT. Surface modification of covalently amine-attached carbon-based magnetic nanoparticles (CMNs) can be produced quite simply in submerged arc discharge using the amine-containing liquid medium ethylenediamine (ED), resulting in CMNs-ED. However, after the arc discharge processing, the resulting nanoparticles possibly contain physically absorbed amine-containing molecules from a liquid medium on the particle surface. To remove the non-covalently bound molecules, a purification process is required. In this study, the purification was conducted using polar and non-polar solvents following the synthesis process. The surface property was initially characterized by a dispersion test in water, showing that CMNs-ED purified by water have better dispersion than CMNs produced in ethanol alone, CMNs-ED before purification, and CMNs-ED after purification by immersion in toluene. Before and after purification, the diffraction pattern showed definitive peaks corresponded to the crystal planes of C(002), Fe_3C(220), and Fe_3O_4(311) at 26.51°, 44.65°, and 35.42°, respectively. The amine functional group on the nanoparticles before purification thought to come from decomposed ethylenediamine assigned by the vibration peaks appeared at a wavenumbers ~3400 cm^{-1} and 1020-1220 cm^{-1}, which corresponds to N-H and C-N, respectively. After purification, the vibration peaks of amine groups were still observable, indicating that the amine groups were still covalently attached to the nanoparticles. Magnetic analysis showed that CMNs before and after purification have superparamagnetic properties, with the magnetic saturation value around 10-17 emu/g. The electron microscope images show that the CMNs-ED before purification have a spherical form with a diameter larger than CMNs-ED after purification.

Keywords: carbon, magnetic nanoparticle, submerged arc discharge, ethylenediamine, purification

INTRODUCTION

Magnetic nanoparticles are the most interesting and exciting material to be developed this decade. Magnetic nanoparticles have unique chemical and physical properties, such as small size, large surface-to-volume ratio, easy synthesis and functionalization, and good biocompatibility (Huang, Lu, & Yang, 2019). These properties offer unique opportunities for many applications, such as adsorption of heavy metal ions from industrial wastewater (Almomani, Bhosale, Khraisheh, Kumar, & Almomani, 2020; Liu et al., 2020), serving as a catalyst (Javadi, Zareyee, Monfared, Didehban, & Mirshokraee, 2020; Maleki, Taheri-Ledari, Ghalavand, & Firouzi-Haji, 2020), or in Li-ion batteries (Moradi, Wang, & Botte, 2020), biomedicine (Kiplagat, Martin, Onani, & Meyer, 2020; Suleman & Riaz, 2020), and drug delivery (Azizi, Nosrati, & Danafar, 2020; Zhang et al., 2020). One of the most frequently used magnetic nanoparticles is iron. However, because iron can be easily oxidized, thus further reducing its magnetism, it is necessary to case the iron with another material that can inhibit further oxidation, such as graphite. Graphite has inert characteristics, low toxicity, stable mechanical and thermal properties, and biocompatibility (Du et al., 2014). The other compound containing iron with magnetic properties is the iron oxide of Fe_3O_4, which has been proven to be biocompatible in bio-applications, especially when combined with carbon material (Fang, Cheng, Zhang, Zhang, & Keidar, 2018; Wang et al., 2018).

Some methods that have been used to synthesize iron oxide/carbon (Fe_3O_4/C)-based materials include the solvothermal method (Ren, Lin, Meng, & Zhang, 2019; Vinodhkumar et al., 2020), the hydrothermal method (Li et al., 2019), and the arc discharge method (Peggiani et al., 2020; Saraswati, Retnosari, Hayati, Amalia, & Hastuti, 2018; Zhao et al., 2019). In general, the arc discharge method can be performed in both a low-pressure chamber and in a liquid medium. The arc discharge method conducted in a liquid medium has several advantages: the relatively short processing time, the simple tools required, and easier purification that yields a high product purity (Sano et al., 2002). Moreover, the submerged arc discharge can easily provide the functionalized

product with specified characteristics for the desired application.

One way to achieve functionalization is by adding the functional groups on the particle surface. For its application in biomedicine, functionalization can be carried out by adding amino groups (Gojny, Nastalczyk, Roslaniec, & Schulte, 2003; Saraswati, Ogino, & Nagatsu, 2012). The magnetic nanoparticles produced are generally hydrophobic; however, the hydrophobic characteristic can be changed to hydrophilic by amino groups' attachment on surface particles. Furthermore, the functionalization using amino groups improves dispersion and increases interfacial interaction between nanoparticles and the functional group (Gojny et al., 2003).

In the submerged arc discharge, surface nanoparticles with functional groups can be modified by replacing the liquid medium with protic and hydrophilic functional groups. This technique has been already developed by Saraswati et al. using the addition of ammonia for surface functionalization (Saraswati, Astuti, & Rismana, 2018). Furthermore, they also used additional ethylenediamine for surface modification of the nanoparticle (Rismana, Astuti, Suselo, Anwar, & Saraswati, 2018).

However, the purity of the product produced is also considered important. The by-product commonly formed in submerged arc discharge is amorphous carbon; thus, the amorphous carbon and other impurities need to be removed. Demonstrations of the various purification methods of carbon nanomaterial have frequently been published for CNTs (Hou, Liu, & Cheng, 2008). Several purification methods for carbon nanotubes (CNTs) have been reported (Hou et al., 2008), including by filtration (Bandow et al., 1997) and centrifugation (Yu et al., 2006). The centrifugation method is an efficient and low-cost method for the purification of carbon materials (Deng et al., 2009). Another technique for purification uses an annealing method (Li et al., 2012). The annealing method was also reported to remove impurities with high effectiveness using vacuum and thermal methods (Meyer-Plath et al., 2012).

In this work, we synthesized CMNs nanoparticles with the arc discharge method in a liquid medium of ethylenediamine mixed with ethanol to modify the particle surface with amine groups followed by the purification process using a combined purification technique by dissolving impurities in organic solvents, annealing, and centrifugation. To the best of our knowledge, the analysis of physical and chemical properties of CMNs before and after purification, including the detail of the changing characteristics influenced by purification in each step, have not been reported elsewhere. These modified techniques considerably improved the purity of the product. The effect of purification on the nanoparticle structure was investigated using X-ray diffraction (XRD), Fourier transform infrared (FTIR), scanning electron microscope-energy dispersive X-Ray (SEM-EDX), vibrating sample magnetometer (VSM), and transmission electron microscopy (TEM). The other characteristics of nanoparticles, such as magnetism and hydrophilicity after purification, were also investigated by simple tests with a magnetic bar and a dispersion test in distilled water, respectively.

EXPERIMENTAL SECTION

Materials

The materials used are a graphite rod and graphite tube from Qingdao Tenry Cardon Co. Ltd (carbon 99%; density 1.95 g/cm^3; electrical resistance 7-10 ohm; graphite rod dimension: d = 10 mm, l = 50 mm), iron oxide (Fe_3O_4) (technical grade), graphite powder (Merck, molar mass of 12.01 g/mol), fructose binder (technical grade, Rosebrand), distilled water, ethanol 70% (technical grade), and ethylenediamine (Merck, >99.9%).

Synthesis of Ethylenediamine-Modified Carbon Magnetic Nanoparticles (CMNs-ED)

As an anode, the modified graphite electrode was filled with a mixture of Fe_3O_4, carbon powder, and fructose binder in a 1:3:2 ratio (w/w/w). The modified electrode was heated at 250 °C under vacuum conditions for six hours. CMNs were prepared with the arc discharge method using 300 mL ethanol 50%. Meanwhile, for the CMNs-ED preparation, ethanol with ethylenediamine addition (50%:50%) in 300 mL total volume was used as a liquid medium of the arc discharge. The process was carried out using 20 V and 10 A of current. Each arc process was continued for about 2 minutes. After arc discharge terminated, the CMNs-ED were collected from the liquid medium by centrifugation and decantation. The heating treatment at 150 °C was then applied to get dried CMNs-ED as a product.

Purification of Ethylenediamine-Modified Carbon Magnetic Nanoparticles (CMNs-ED)

We compared several purification techniques as follows. The first purification technique was carried out by washing the collected nanoparticles using distilled water several times. The water and the nanoparticles were separated by centrifugation. After the supernatant was discharged, the sediment, or product, was dried at 150 °C. CMNs dried in this stage were named CMNs-ED purified by water. The next purification technique was the continuation of the previous stage. CMNs-ED purified by water were annealed by utilizing a thermal vacuum annealed in horizontal tubular furnaces at a temperature of 250 °C and a heating rate of 5 °C/min for six hours. CMNs dried in this stage were named CMNs-ED purified by annealing. A further purification step was conducted by immersing CMNs-ED annealed in the previous stage in toluene for 24 h, followed by annealing treatment at 250 °C. CMNs dried in this stage were

named CMNs-ED purified by immersion in toluene, followed by annealing treatment.

Dispersity and Magnetic Tests

The magnetization and dispersion tests were used to determine the magnetic response and the surface characteristics of CMNs-ED nanoparticles, respectively. The dispersity test was done by mixing 0.01 gram of nanoparticles in distilled water and was then continued by sonication for 15 minutes. Dispersion testing was carried out by observing the mixture after sonication 60s and 1h. Magnetic tests were carried out by using a magnetic bar. The test was analyzed by observing the attractivity response of the magnetized nanoparticles.

Characterization of the Materials

The products of each phase were investigated using X-ray diffraction (XRD) (Philips X'pert Pro; Cu-Kα source λ = 1.54060 Å, step = 0.017°; range = 5-80°). The structural properties of CMNs-ED were studied using transmission electron microscopy (TEM) (FEI Tecnai G2 20 S-Twin; 200kV voltage acceleration class; sub angstrom resolution of 0.24 nm (point) and 0.188 nm (line); magnification range of ×30.0k). The CMNs-ED particle size distribution before and after purification was estimated based on the diameter data of nanoparticles measured by the ImageJ application. The infrared spectra measured by Fourier transform infrared (FTIR) (Shimadzu IR Prestige-21; range = 500 and 4000 cm^{-1}; KBr pellet) were used to analyze attached functional groups. Further characterizations were also performed using a scanning electron microscope (SEM) (Hitachi SU-3500; widescreen GUI; Ultra Variable-Pressure Detector) and vibrating sample magnetometer (VSM) (VSM250; T= 298-773 K; external magnetic field [H = 100 Oe-21 kOe]) to analyze the morphological structure and the magnetic property of the nanoparticles, respectively.

RESULTS AND DISCUSSION

The differences of the surface characteristics of the CMNs before and after purification, including with and without ED addition, were easily recognized by dispersing CMNs in distilled water, as shown in **Figure 1**. A through E in **Figure 1** respectively correspond to CMNs, CMNs-ED before purification, CMNs-ED purified by water, CMNs-ED purified by annealing, and CMNs-ED purified by immersion in toluene followed by annealing treatment. The results of the dispersion test were carried out under four conditions, namely before sonication (**A1-E1**), just after sonication (**A2-E2**), after being allowed to settle for 60s (**A3-E3**), and 1h (**A4-E4**). Before sonication, the unmodified nanoparticles CMNs had a hydrophobic character (**A1**). The effect of functionalization using the amine group caused CMNs, which were initially hydrophobic, to become hydrophilic. The purification also affected the color of the dispersion liquid produced. Before purification, the dispersion liquid was yellowish, which is thought to be due to excess ethylenediamine in the arc discharge product (**B1**). On the other hand, the purification using distilled water removed the remained ethylenediamine, producing a clear dispersion liquid (**C1-E1**).

Figures 1 (**A2-E2**) show the CMNs dispersion just after sonication, which indicates that sonication treatment can be used to improve the dispersion of the nanoparticles. The nanoparticle dispersion test's stability was confirmed 60 s after sonification whether the nanoparticles were settling or not, as shown in **Figures 1** (**A3-E3**). In **Figure 1** (**A3**), even though the sonication treatment had been performed, the CMNs nanoparticles remained in a non-dispersible form in water, shown as floating particles above the water due to the absence of the hydrophilic functional groups. On the other hand, as shown in **Figures 1** (**B3-E3**), the nanoparticles have good dispersion stability after 60s.

Figure 1(**A4**) shows that after one hour of settling, CMNs return to float on the water as in the initial dispersion state. In the **Figures 1** (**B4** and **D4**), the nanoparticles also began to fall and settle. Interestingly, the nanoparticles shown in **Figure 1** (**C4**) have the best dispersion stability due to the influence of the successful surface modification with amine groups. **Figure 1**(**E4**) shows that the dispersion of CMNs-ED in water is worse after purification treatment with toluene. The toluene may physically be absorbed on the CMNs-ED nanoparticles, resulting in the hydrophobic characteristics on the nanoparticle surface triggering the worst dispersity, which accords with the work reported by Tasca et al. (Tasca, Ghajeri, & Fletcher, 2017).

The functional groups present in CMNs-ED before purification, CMNs-ED purified by water, CMNs-ED purified by annealing, and CMNs-ED purified by immersion in toluene followed by annealing treatment were further analyzed by FTIR spectroscopy, as shown in **Figure 2**. CMNs produced without ED added were not further analyzed using FTIR because the surface characteristics could already be significantly seen from the dispersion properties in **Figure 1**. For CMNs produced with ED added, the characterization using FTIR was analyzed to study the effect of the purifications and the amine groups, which possibly attached to the nanoparticles' surface. The FTIR results featured in **Figure 2** present information about the presence of O−H, N−H, C=C, C−H, C−OH, Fe−O summarized in detail in **Table 1**. FTIR analysis was used to compare the effect of purifications on the functional groups of nanoparticles. Free O−H (A) was observed at wavenumber 3600-3700 cm^{-1} (Saraswati, Retnosari, Hayati, Amalia, & Hastuti, 2018). The FTIR spectra after purification are shown in **Figure 2** (**b-d**). The absorption of O-H stretching decreases, which indicates the decreasing H_2O vavor content in nanoparticles due to the purification effect, especially from the annealing method.

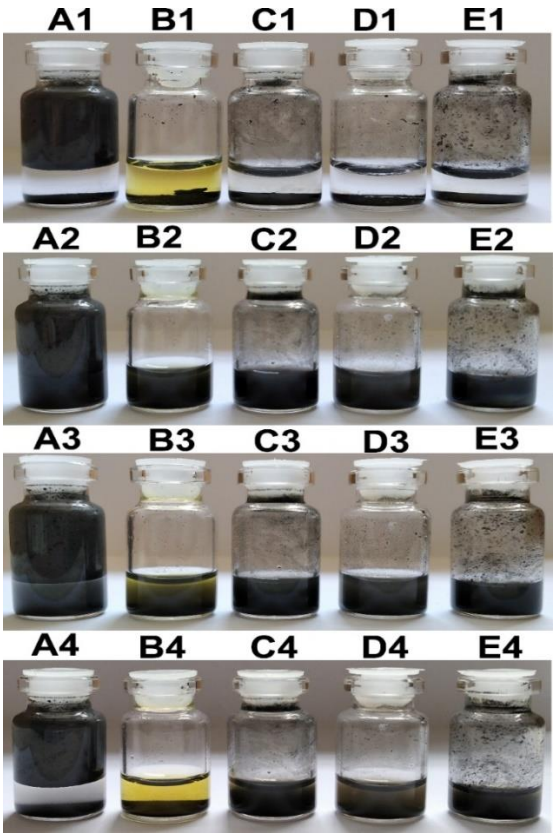

Figure 1. Dispersion tests of (**A**) CMNs synthesized without ED added, (**B**) CMNs-ED before purification, (**C**) CMNs-ED purified by water, (**D**) CMNs-ED purified by annealing, and (**E**) CMNs-ED purified by immersing in toluene followed by annealing treatment. The results of the dispersion test were carried out under different conditions, namely (**A1-E1**) before sonication, (**A2-E2**) just after sonication, (**A3-E3**) continuously settling after 60s, and (**A4-E4**) settled after 1h.

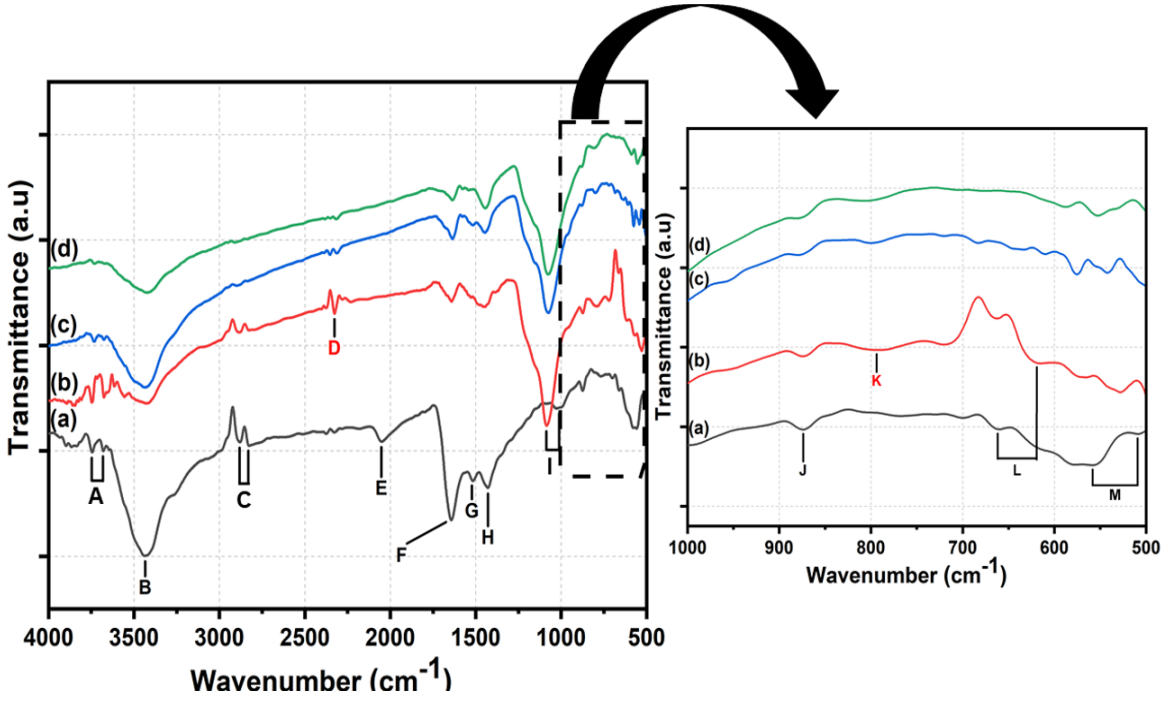

Figure 2. FTIR spectra of continuous steps of purification of CMNs-ED: (**a**) CMNs-ED before purification, (**b**) CMNs-ED purified by water, (**c**) CMNs-ED purified by annealing, and (**d**) CMNs-ED purified by immersion in toluene followed by annealing treatment. A to M are explained in detail in **Table 1**.

Table 1. The summary of FTIR assignments according to the spectra presented in **Figure 2**.

Peak	Wavenumber (cm^{-1})				References	
	Spectrum (**a**)	Spectrum (**b**)	Spectrum (**c**)	Spectrum (**d**)	Wavenumber According to Ref. (cm^{-1})	Assignments
A	3745	3744	3731	3732	~3600-3700 (Saraswati et al., 2018)	O−H free
	3679	3675	3676	-		
B	3437	3435	3437	3423	~3400 (Ajmal, Yunus, Matin, & Haq, 2015; Avedian, Zaaeri, Daryasari, Javar, & Khoobi, 2018)	N−H
C	2882	2888	2896	2908	~2900 (Seifan, Ebrahiminezhad, Ghasemi, Samani, & Berenjian, 2018; Vieira et al., 2020)	C−H stretching
	2831	2828	2830	2835		
D	2325	2325	2313	2314	2200-2450 (Stuart, 2004)	Combination C−H stretching
E	2051	-	-	-	2000-2200 (Stuart, 2004)	Combination N−H stretching or O−H stretching
F	1642	1639	1635	1632	~1645 (Ramanathan, Fisher, Ruoff, & Brinson, 2005)	NH_2 primary amine
G	1518	1525	1526	-	1539 (Olad & Bakht Khosh Hagh, 2019)	N−H bending
H	1430	1441	1434	1435	~1430 (Vieira et al., 2020)	C−H stretching
I	1025	1086	1076	1075	1020-1220 (Stuart, 2004)	C−N stretching
J	873	873	879	873	873 (Karimzadeh et al., 2017)	C=C
K	-	793	797	799	775-850 (Stuart, 2004)	Overtone N−H stretching
L	661	663	682	-	600-700 (Stuart, 2004)	O−H bending
	-	619	612	-		
M	558	572	576	586	~578 (Mohapatra, Mitra, Bahadur, & Aslam, 2013)	Fe−O
	509	528	542	553		

The absorption of the N−H bond was observed at a wavenumber ~3400 cm^{-1} (B) (Ajmal et al., 2015; Avedian et al., 2018). Before purification, the CMNs-ED show a peak at 3437 cm^{-1} (B) with strong intensity, as shown in **Figure 2**(**a**), which is thought to correspond to the excess of ethylenediamine. The purification might decrease the intensity of the N-H stretch bend. This phenomenon suggests that the purification decreases the physical bonding between the N-H in ethylenediamine and the C atom in the carbon nanomaterials' surface. The vibrations of the N−H bond were observed at wavenumber ~1645 cm^{-1}, ~1500 cm^{-1}, and 775-850 cm^{-1} (Ramanathan et al., 2005; Stuart, 2004). The peak observed at wavenumber ~1645 cm^{-1} (F) is the primary amine of NH_2 groups (Ramanathan et al., 2005), which is thought to indicate the absorption of primary amine NH_2 attached to the carbon. The purification effect triggered the primary amine decrease on the surface of the nanoparticles. The absorption at wavenumbers around 1020-1220 cm^{-1} (I) was detected as C-N bond stretching vibrations (Ramanathan et al., 2005; Stuart, 2004). A band at 1025 cm^{-1} (**Figure 2a**) (I) indicates the presence of C−N, which suggests that the functionalization of nanoparticles with ethylenediamine resulting in the covalent attachment of amine groups to the C atom was achieved. After purification (see **Figures 2**(**b-d**)), the C−N bond

intensity was stronger than before purification. An increase in the peak intensity generally means an increase in the functional group's number. The absorption band of C−N after purification created a spectral shift that occurred in 1086 cm^{-1}, 1076 cm^{-1}, and 1075 cm^{-1}, as shown in **Figures 2**(**b-d**), respectively. The peak at 540-590 cm^{-1} (M) is attributed to the stretching vibrations of the Fe-O (Fe^{3+} bond) of Fe_3O_4 in octahedral sites (Baye, Abebe, Appiah-Ntiamoah, & Kim, 2019; Li, Wu, Li, Tang, & Chen, 2018). Before purification, the absorption of Fe−O had a strong intensity; however, after purification, the intensity of Fe−O was decreased. The decrease of Fe-O intensity is further analyzed in the discussion of diffraction data.

To study the purification effect on the crystalline phase, CMNs-ED nanoparticles before and after purification were analyzed by using XRD equipment. The diffraction patterns for CMNs-ED before purification, CMNs-ED purified by water, and CMNs-ED purified by immersion in toluene followed by annealing method are shown in **Figure 3**. Due to the similar surface characteristics of CMNs-ED purified in the second stage with CMNs-ED purified by annealing, as shown in **Figures 1** and **2**, this sample was not further characterized by XRD.

The XRD results show that CMNs-ED synthesized by the arc discharge method have typical diffraction peaks at 2θ 26.51° and 77.43°, correspond to Miller indices of graphite carbon (002) and (110), which is in agreement with the typical diffraction pattern of carbon in accordance with PDF #41-1487. The diffraction peaks around 29.45°, 44.65°, and 54.67° correspond with the (111), (220), and (040) crystal planes of iron carbides (PDF# 77-0255). The characteristic peaks at 2θ of 35.42°, 43.05°, 56.98°, and 62.51° are consistent with the crystal planes of Fe_3O_4 (311), (400), (511), and (440), respectively. In addition, the diffraction peak at 30.01° is confirmed to be Fe_2O_3 assigned to the crystal plane of Fe_2O_3 (220).

Before purifications, the peaks of Fe_3O_4 had a strong intensity; however, after purification with annealing, as shown in **Figures 3**(**b**) and (**c**), the intensity of Fe_3O_4 decreased. The annealing method carried out under vacuum conditions minimized the presence of oxygen. Under limited oxygen conditions, oxygen present in Fe_3O_4 will decrease, which is in line with EDX data. Therefore, the reaction with other elements than oxygen, e.g., carbon, occurred more, resulting in the greater dominance of iron carbide as indicated by the increasing intensity of the peak at 2θ 54.67° as Fe_3C (040). This phenomenon shows that the purification has omitted the Fe_3O_4. The effect of purification also decreased the intensity of Fe_3O_4 and Fe_2O_3, suggesting that it influences the magnetization of the purified products. Moreover, the purification effect of CMNs-ED impacts the reduced intensity of the amorphous carbon diffraction peak at 2θ 21.36° (Shi et al., 2015).

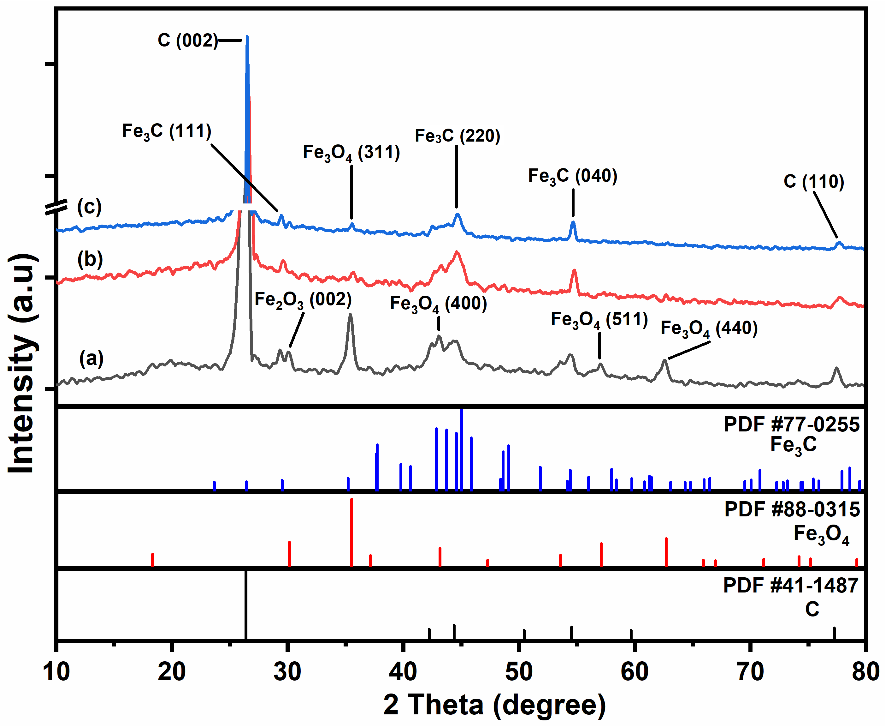

Figure 3. XRD diffractogram of the steps of purification of CMNs-ED: (**a**) CMNs-ED before purification, (**b**) CMNs-ED purified by water, and (**c**) CMNs-ED purified by immersion in toluene followed by annealing treatment.

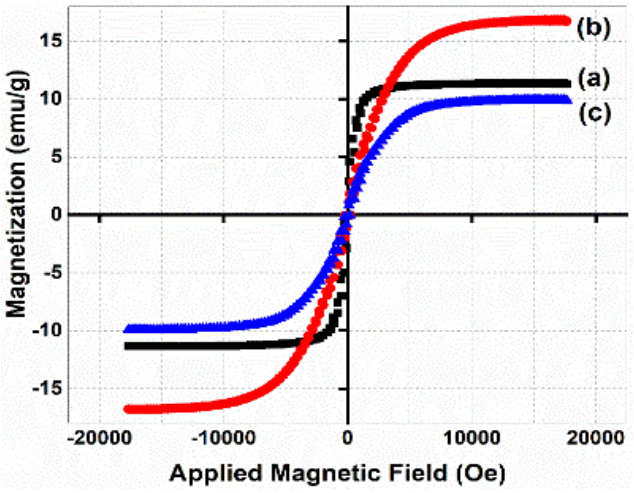

Figure 4. Magnetization curve of (**a**) CMNs-ED before purification, (**b**) CMNs-ED purified by water, and (**c**) CMNs-ED purified by immersion in toluene followed by annealing treatment.

The magnetic property of CMNs-ED before purification, CMNs-ED purified by water, and CMNs-ED purified by immersion in toluene followed by annealing treatment was investigated with a vibrating sample magnetometer (VSM). The magnetization curve of the samples was measured at room temperature, as shown in **Figure 4**. The magnetization curve shows that the magnetic saturation (M_s) value of CMNs-ED before purification, CMNs-ED purified by water, and CMNs-ED purified by immersion in toluene followed by annealing treatment are 11.38 emu/g, 16.87 emu/g, and 9.95 emu/g, respectively. Saturation magnetization is a primary factor for successful magnetic separation. According to the previous study, the magnetic saturation value >10 emu/g was enough for magnetic separation from the aqueous solution using an external magnetic bar (Dhoble, Lunge, Bhole, & Rayalu, 2011; Ma, Guan, & Liu, 2005). The hysteresis profiles have completely reversible S-shapes. These data confirmed that the superparamagnetic characteristics were maintained in the CMNs-ED before and after the purification process.

The magnetization test was also carried out by magnet attraction. The visible magnetic testing results are shown in **Figure 5**, which presents the CMNs-ED before purification, CMNs-ED purified by water, and CMNs-ED purified by immersion in toluene followed by annealing treatment. The products in powdery form and dispersed in distilled water are shown to be magnetic and attractable to the magnet. Therefore, the purification presented in this study give no effect on the magnetism attractions visually shown in **Figure 5**.

Figures 6(**a–d**) show the SEM image of CMNs-ED before purification, CMNs-ED purified by water, CMNs-ED purified by annealing, and CMNs-ED purified by immersion in toluene followed by annealing treatment. As shown in **Figures 6**(**a-b**), the product's surface consists of grains and layer, suggesting that the Fe_3O_4 particles are attached to the carbon layers. As shown in **Figures 6**(**c-d**), the nanoparticles' surface is covered by granular particles densely distributed on the surface probably as Fe_3O_4.

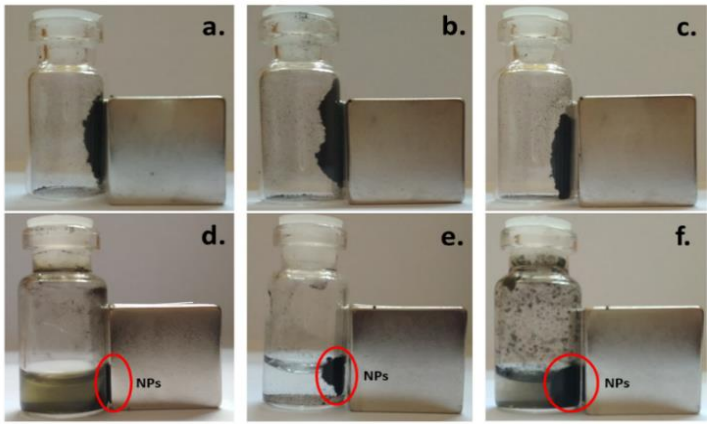

Figure 5. The magnetism of (**a,d**) CMNs-ED before purification, (**b,e**) CMNs-ED purified by water, and (**c,f**) CMNs-ED purified by immersion in toluene followed by annealing treatment. Interactions NPs with a magnet (upper) and interactions NPs in distilled water by using an external magnetic bar (lower).

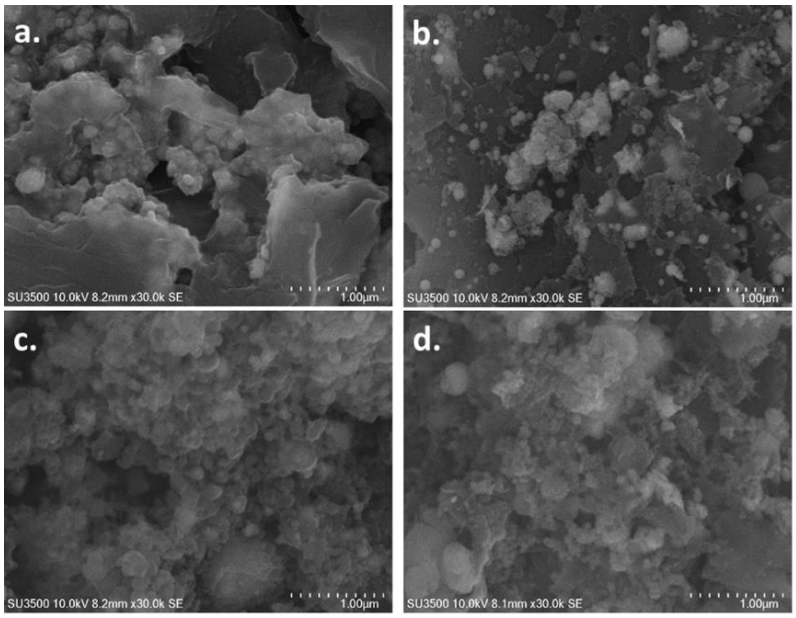

Figure 6. SEM images of (**a**) CMNs-ED before purification, (**b**) CMNs-ED purified by water, (**c**) CMNs-ED purified by annealing, and (**d**) CMNs-ED purified by immersion in toluene followed by annealing treatment.

Table 2. EDX results of CMNs-ED before purification, CMNs-ED purified by water, CMNs-ED purified by annealing, and CMNs-ED purified by immersion in toluene followed by annealing treatment.

Sample	Weight Percentage (%)			
	C	Fe	O	N
CMNs-ED before purification	60.84	9.23	16.77	13.16
CMNs-ED purified by water	72.56	9.66	11.28	6.49
CMNs-ED purified by annealing	54.4	27.48	9.59	4.7
CMNs-ED purified by immersing in toluene followed by annealing treatment	74.61	11.06	8.56	3.72

The elemental analysis of the EDX data of CMNs-ED before purification, CMNs-ED purified by water, CMNs-ED purified by annealing, and CMNs-ED purified by immersion in toluene followed by annealing treatment is shown in **Table 2**. The SEM-interpreted data was correlated with the elemental analysis of Fe. As shown in **Table 2**, the weight percentages of Fe atoms in CMNs-ED purified by annealing and CMNs-ED purified by immersing in toluene followed by annealing treatment are 27.48 and 11.06, respectively. This weight percentage of Fe contributed to Fe_3O_4 and Fe_3C. On the other hand, the purifications possibly caused the decreased weight percentage of elements O and N.

The TEM images of CMNs-ED before purification, CMNs-ED purified by water, CMNs-ED purified by annealing, and CMNs-ED purified by immersion in toluene followed by annealing treatment are respectively shown in **Figures 7**(**a-d**). The results show that purification affects the nanoparticles' structure and morphology. **Figure 7**(**a**) shows that iron compounds which are possibly dominant as Fe_3O_4 particles (according to XRD analysis) — due to the content of metal elements — represented as a darker area are relatively larger than those of particles in the other TEM images [see **Figures 7**(**b-d**)] that are located outside of the carbon layers.

Figure 7(**b**) shows the structure and morphology of CMNs-ED purified by water. As can be seen in **Figure 7**(**b**), the nanoparticles CMNs-ED were not agglomerated. After the purification, the large particles are reduced. The smaller iron compounds are left behind trapped in the carbon layer, rendering the nanoparticles hard to lose. **Figure 7**(**c**) shows the structure and morphology of CMNs-ED purified by annealing. The results indicated that **Figure 7**(**c**) is almost the same as **Figure 7**(**b**) in a specific area. Additionally, the carbon layers were observed with less amorphous carbon in some areas. The TEM images of nanoparticles CMNs-ED purified by immersion in toluene followed by annealing treatment (**Figure 7d**) indicated that the Fe_3O_4 was wrapped in the carbon layers, even though in some areas they only show the carbon layers. In general, purification with any method performed in this study confirms the characteristics of particles produced as iron compounds — according to XRD data, these compounds are likely to be Fe_3O_4 and dominant Fe_3C — wrapped by carbon layers. The CMNs-ED before purification has a slightly larger size than CMNs-ED after purification.

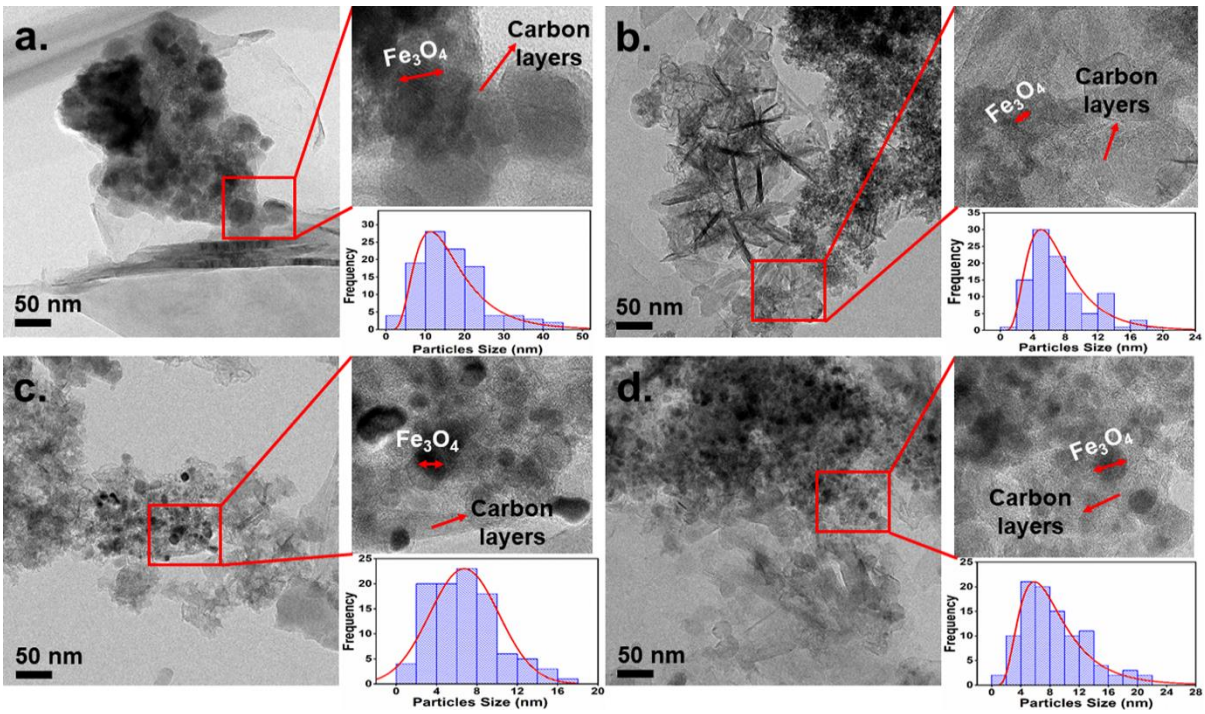

Figure 7. TEM images and histogram of particles size of (**a**) CMNs-ED before purification, (**b**) CMNs-ED purified by water, (**c**) CMNs-ED purified by annealing, and (**d**) CMNs-ED purified by immersion in toluene followed by annealing treatment.

CONCLUSIONS

Amine-modified CMNs were successfully synthesized by submerged arc discharge in ethylenediamine. Hence the dispersion test of CMNs produced in submerged arc discharge with and without ethylenediamine addition shows different characteristics. Several purification steps performed in this study variously affect dispersity, in which purification using water with sonication is revealed to be the better purification method compared to the others. The XRD diffractogram of CMNs-ED reveals the main characteristics of carbon, Fe_3C, and Fe_3O_4. Additionally, the purification conducted in this study reduces the intensity of Fe_3O_4 and increases the crystalline peaks of carbide Fe_3C. FTIR analysis indicates that the amine group was successfully attached, indicated by C-N peaks observable at wavenumber 1020-1220 cm^{-1}. The CMNs-ED before purification have a dominant particle size of 10-15 nm. The structure of CMNs-ED after purification was observed as an iron compound wrapped by carbon layers with the dominant particle size less than 10 nm. After purification, the magnetism of nanoparticles remained, as confirmed by powder's attraction to the magnet and by the hysteresis loop analyzed using VSM showing the CMNs magnetization at ~10 emu/g.

ACKNOWLEDGEMENTS

The author would like to thank the Ministry of Research and Technology/National Agency for Research and Innovation, the Republic of Indonesia for finacial support under Project No. 719/UN27.21/PN/2019 and 112/UN27.21/HK/2020.

REFERENCES

Ajmal, M., Yunus, U., Matin, A., & Haq, N. U. (2015). Synthesis, characterization and in vitro evaluation of methotrexate conjugated fluorescent carbon nanoparticles as drug delivery system for human lung cancer targeting. *Journal of Photochemistry and Photobiology B: Biology, 153*, 111-120. doi:https://doi.org/10.1016/j.jphotobiol.2015.09.006

Almomani, F., Bhosale, R., Khraisheh, M., Kumar, A., & Almomani, T. (2020). Heavy metal ions removal from industrial wastewater using magnetic nanoparticles (MNP). *Applied Surface Science, 506*, 144924. doi:https://doi.org/10.1016/j.apsusc.2019.144924

Avedian, N., Zaaeri, F., Daryasari, M. P., Akbari Javar, H., & Khoobi, M. (2018). pH-sensitive biocompatible mesoporous magnetic nanoparticles labeled with folic acid as an efficient carrier for controlled anticancer drug delivery. *Journal of Drug Delivery Science and Technology, 44*, 323-332. doi:https://doi.org/10.1016/j.jddst.2018.01.006

Azizi, S., Nosrati, H., & Danafar, H. (2020). Simple surface functionalization of magnetic nanoparticles with methotrexate-conjugated

bovine serum albumin as a biocompatible drug delivery vehicle. *Applied Organometallic Chemistry, 34*(4), e5479. doi:10.1002/aoc.5479

Bandow, S., Rao, A. M., Williams, K. A., Thess, A., Smalley, R. E., & Eklund, P. C. (1997). Purification of Single-Wall Carbon Nanotubes by Microfiltration. *The Journal of Physical Chemistry B, 101*(44), 8839-8842. doi:10.1021/jp972026r

Baye, A. F., Abebe, M. W., Appiah-Ntiamoah, R., & Kim, H. (2019). Engineered iron-carbon-cobalt (Fe_3O_4@C-Co) core-shell composite with synergistic catalytic properties towards hydrogen generation via $NaBH_4$ hydrolysis. *Journal of colloid and interface science, 543*, 273-284. doi:https://doi.org/10.1016/j.jcis.2019.02.065

Deng, X., Xiong, D., Wang, H., Chen, D., Jiao, Z., Zhang, H., & Wu, M. (2009). Bulk enrichment and separation of multi-walled carbon nanotubes by density gradient centrifugation. *Carbon, 47*(6), 1608-1610. doi:https://doi.org/10.1016/j.carbon.2009.02.016

Dhoble, R. M., Lunge, S., Bhole, A. G., & Rayalu, S. (2011). Magnetic binary oxide particles (MBOP): A promising adsorbent for removal of As (III) in water. *Water research, 45*(16), 4769-4781. doi:https://doi.org/10.1016/j.watres.2011.06.016

Du, Y., Liu, W., Qiang, R., Wang, Y., Han, X., Ma, J., & Xu, P. (2014). Shell Thickness-Dependent Microwave Absorption of Core–Shell Fe_3O_4@C Composites. *ACS applied materials & interfaces, 6*(15), 12997-13006. doi:10.1021/am502910d

Fang, X., Cheng, X., Zhang, Y., Zhang, L. G., & Keidar, M. (2018). Single-step synthesis of carbon encapsulated magnetic nanoparticles in arc plasma and potential biomedical applications. *Journal of colloid and interface science, 509*, 414-421. doi:https://doi.org/10.1016/j.jcis.2017.09.015

Gojny, F. H., Nastalczyk, J., Roslaniec, Z., & Schulte, K. (2003). Surface modified multi-walled carbon nanotubes in CNT/epoxy-composites. *Chemical Physics Letters, 370*(5), 820-824. doi:https://doi.org/10.1016/S0009-2614 (03) 00187-8

Hou, P.-X., Liu, C., & Cheng, H.-M. (2008). Purification of carbon nanotubes. *Carbon, 46*(15), 2003-2025. doi:https://doi.org/10.1016/j.carbon.2008.09.009

Huang, G., Lu, C.-H., & Yang, H.-H. (2019). Chapter 3 - Magnetic Nanomaterials for Magnetic Bioanalysis. In X. Wang & X. Chen (Eds.), *Novel Nanomaterials for Biomedical, Environmental and Energy Applications* (pp. 89-109): Elsevier.

Javadi, S. H., Zareyee, D., Monfared, A., Didehban, K., & Mirshokraee, S. A. (2020). Silica-coated Fe_3O_4 magnetic nanoparticles-supported sulfonic acid as a highly active and reusable catalyst in chemoselective deprotection of tert-butyldimethylsilyl (TBDMS) ethers. *Phosphorus, Sulfur, and Silicon and the Related Elements, 195*(1), 7-12. doi:10.1080/10426507.2019.1576680.

Karimzadeh, I., Aghazadeh, M., Doroudi, T., Ganjali, M. R., Kolivand, P. H., & Gharailou, D. (2017). Amino Acid Coated Superparamagnetic Iron Oxide Nanoparticles for Biomedical Applications Through a Novel Efficient Preparation Method. *Journal of Cluster Science, 28*(3), 1259-1271. doi:10.1007/s10876-016-1139-z

Kiplagat, A., Martin, D. R., Onani, M. O., & Meyer, M. (2020). Aptamer-conjugated magnetic nanoparticles for the efficient capture of cancer biomarker proteins. *Journal of Magnetism and Magnetic Materials, 497*, 166063. doi:https://doi.org/10.1016/j.jmmm.2019.166063

Li, L., Wang, T., Zhang, L., Su, Z., Wang, C., & Wang, R. (2012). Selected-Control Synthesis of Monodisperse Fe_3O_4@C Core–Shell Spheres, Chains, and Rings as High-Performance Anode Materials for Lithium-Ion Batteries. *Chemistry – A European Journal, 18*(36), 11417-11422. doi:10.1002/chem.201200791

Li, L., Wang, X., Ma, Z., Liu, L., Wang, H., Zhang, W., & Li, X. (2019). Electrospinning synthesis and electrocatalytic performance of iron oxide/carbon nanofibers composites as a low-cost efficient Pt-free counter electrode for dye-sensitized solar cells. *Applied Surface Science, 475*, 109-116. doi:https://doi.org/10.1016/j.apsusc.2018.2.150

Li, W., Wu, X., Li, S., Tang, W., & Chen, Y. (2018). Magnetic porous Fe_3O_4/carbon octahedra derived from iron-based metal-organic framework as heterogeneous Fenton-like catalyst. *Applied Surface Science, 436*, 252-262. doi:https://doi.org/10.1016/j.apsusc.2017.11.151

Liu, X., Guan, J., Lai, G., Xu, Q., Bai, X., Wang, Z., & Cui, S. (2020). Stimuli-responsive adsorption behavior toward heavy metal ions based on comb polymer functionalized magnetic nanoparticles. *Journal of Cleaner Production, 253*, 119915. doi:https://doi.org/10.1016/j.jclepro.2019.119915

Ma, Z., Guan, Y., & Liu, H. (2005). Synthesis and characterization of micron-sized monodisperse superparamagnetic polymer particles with amino groups. *Journal of Polymer Science Part A: Polymer Chemistry, 43*(15), 3433-3439. doi:10.1002/pola.20803

Maleki, A., Taheri-Ledari, R., Ghalavand, R., & Firouzi-Haji, R. (2020). Palladium-decorated o-phenylenediamine-functionalized Fe_3O_4/SiO2 magnetic nanoparticles: A promising solid-state catalytic system used for Suzuki–Miyaura coupling reactions. *Journal of Physics and Chemistry of Solids, 136*, 109200. doi:https://doi.org/10.1016/j.jpcs.2019.109200

Meyer-Plath, A., Orts-Gil, G., Petrov, S., Oleszak, F., Maneck, H.-E., Dörfel, I., . . . Mach, R. (2012). Plasma-thermal purification and annealing of carbon nanotubes. *Carbon, 50*(10), 3934-3942. doi:https://doi.org/10.1016/j.carbon.2012.04.049

Mohapatra, J., Mitra, A., Bahadur, D., & Aslam, M. (2013). Surface controlled synthesis of MFe_2O_4 (M = Mn, Fe, Co, Ni and Zn) nanoparticles and their magnetic characteristics. *CrystEngComm, 15*(3), 524-532. doi:10.1039/C2CE25957E

Moradi, B., Wang, D., & Botte, G. G. (2020). Carbon-coated Fe_3O_4 nanospindles as solid electrolyte interface for improving graphite anodes in lithium ion batteries. *Journal of Applied Electrochemistry, 50*(3), 321-331. doi:10.1007/s10800-019-01393-0

Olad, A., & Bakht Khosh Hagh, H. (2019). Graphene oxide and amin-modified graphene oxide incorporated chitosan-gelatin scaffolds as promising materials for tissue engineering. *Composites Part B: Engineering, 162*, 692-702. doi:https://doi.org/10.1016/j.compositesb.2019.01.040

Peggiani, S., Senis, A., Facibeni, A., Milani, A., Serafini, P., Cerrato, G., . . . Casari, C. S. (2020). Size-selected polyynes synthesised by submerged arc discharge in water. *Chemical Physics Letters, 740*, 137054. doi:https://doi.org/10.1016/j.cplett.2019.137054

Ramanathan, T., Fisher, F. T., Ruoff, R. S., & Brinson, L. C. (2005). Amino-Functionalized Carbon Nanotubes for Binding to Polymers and Biological Systems. *Chemistry of Materials, 17*(6), 1290-1295. doi:10.1021/cm048357f

Ren, L., Lin, H., Meng, F., & Zhang, F. (2019). One-step solvothermal synthesis of Fe_3O_4@Carbon composites and their application in removing of Cr (VI) and Congo red. *Ceramics International, 45*(7, Part B), 9646-9652. doi:https://doi.org/10.1016/j.ceramint.2018.11.132

Rismana, N., Astuti, A. R., Suselo, Y. H., Anwar, M., & Saraswati, T. E. (2018). Preparation of amine-modified Fe_3O_4/carbon nanoparticles by submerged arc discharge in ethylenediamine/ethanol. *IOP Conference Series: Materials Science and Engineering, 333*, 012026. doi:10.1088/1757-899x/333/1/012026

Sano, N., Wang, H., Alexandrou, I., Chhowalla, M., Teo, K. B. K., Amaratunga, G. A. J., & Iimura, K. (2002). Properties of carbon onions produced by an arc discharge in water. *Journal of Applied Physics, 92*(5), 2783-2788. doi:10.1063/1.1498884

Saraswati, T. E., Astuti, A. R., & Rismana, N. (2018). Quantitative analysis by UV-Vis absorption spectroscopy of amino groups attached to the surface of carbon-based nanoparticles. *IOP Conference Series: Materials Science and Engineering, 333*, 012027. doi:10.1088/1757-899x/333/1/012027

Saraswati, T. E., Ogino, A., & Nagatsu, M. (2012). Plasma-activated immobilization of biomolecules onto graphite-encapsulated magnetic nanoparticles. *Carbon, 50*(3), 1253-1261. doi:https://doi.org/10.1016/j.carbon.2011.10.044

Saraswati, T. E., Retnosari, I., Hayati, I. N., Amalia, A., & Hastuti, S. (2018). The Influence of Ammonia Addition on the Surface Characteristics of Fe3O4/Carbon Nanoparticles in Submerged Arc Discharge. *Recent Patents on Materials Science, 11*(2), 71-82. doi:10.2174/1874464812666181128102742

Seifan, M., Ebrahiminezhad, A., Ghasemi, Y., Samani, A. K., & Berenjian, A. (2018). Amine-modified magnetic iron oxide nanoparticle as a promising carrier for application in bio self-healing concrete. *Applied microbiology and biotechnology, 102*(1), 175-184. doi:10.1007/s00253-017-8611-z

Shi, W. P., Liu, W. F., Chen, L., Qin, L., Yang, Y. Z., & Liu, X. G. (2015). Effect of annealing temperature on the structure of carbon encapsulated Fe_3O_4 nanospheres. *RSC Advances, 5*(129), 106787-106794. doi:10.1039/C5RA19326E

Stuart, B. H. (2004). *Infrared Spectroscopy: Fundamentals and Applications*: Wiley.

Suleman, M., & Riaz, S. (2020). In silico study of hyperthermia treatment of liver cancer using core-shell $CoFe_2O_4$@$MnFe_2O_4$ magnetic nanoparticles. *Journal of Magnetism and Magnetic Materials, 498*, 166143. doi:https://doi.org/10.1016/j.jmmm.2019.166143

Tasca, A. L., Ghajeri, F., & Fletcher, A. J. (2017). Novel hydrophilic and hydrophobic amorphous silica: Characterization and adsorption of aqueous phase organic compounds. *Adsorption Science & Technology, 36*(1-2), 327-342. doi:10.1177/0263617417692339

Vieira, L. H. S., Sganzerla Sabino, C. M., Soares Júnior, F. H., Rocha, J. S., Castro, M. O., Alencar, R. S., Ferreira, O P. (2020). Strategic

design of magnetic carbonaceous nanocomposites and its application as multifunctional adsorbent. *Carbon, 161*, 758-771. doi:https://doi.org/10.1016/j.carbon.2020.01.089

Vinodhkumar, G., Wilson, J., Inbanathan, S. S. R., Potheher, I. V., Ashokkumar, M., & Peter, A. C. (2020). Solvothermal synthesis of magnetically separable reduced graphene oxide/Fe_3O_4 hybrid nanocomposites with enhanced photocatalytic properties. *Physica B: Condensed Matter, 580*, 411752. doi:*https://doi.org/10.1016/j.physb.2019.411752*

Wang, H., Mu, Q., Revia, R., Wang, K., Tian, B., Lin, G., . . . Zhang, M. (2018). Iron oxide-carbon core-shell nanoparticles for dual-modal imaging-guided photothermal therapy. *Journal of Controlled Release, 289*, 70-78. doi:https://doi.org/10.1016/j.jconrel.2018.09.022

Yu, A., Bekyarova, E., Itkis, M. E., Fakhrutdinov, D., Webster, R., & Haddon, R. C. (2006). Application of Centrifugation to the Large-Scale Purification of Electric Arc-Produced Single-Walled Carbon Nanotubes. *Journal of the American Chemical Society, 128*(30), 9902-9908. doi:10.1021/ja062041m

Zhang, Z., Zhuang, L., Lin, Y., Yan, M., Lv, J., Li, X., . . . Xu, Y. (2020). Novel drug delivery system based on hollow mesoporous magnetic nanoparticles for head and neck cancers--targeted therapy in vitro and in vivo. *American Journal of Cancer Research, 10*(1), 350-364.

Zhao, J., Luo, J., Li, D., Zhou, Z., Ji, G., Shi, Q., & Xiang, Y. (2019). Fe_3O_4 Nanoparticles Supported on Arc-synthesized Carbon Nanotubes as Advanced Electrocatalyst for Oxygen Reduction Reaction. *ChemistrySelect, 4*(20), 6227-6232. doi:10.1002/slct.201901378